Depositional facies and migration of the eruptive loci for Atexcac axalapazco (central Mexico): implications for the morphology of the crater

Mario López-Rojas* and Gerardo Carrasco-Núñez

Centro de Geociencias, Universidad Nacional Autónoma de México,
Campus Juriquilla, Blvd. Juriquilla No. 3001, C.P. 76230, Querétaro, Qro., México.
** mario_lopr@geociencias.unam.mx*

ABSTRACT

Phreatomagmatic explosions produced an alternated stratified sequence of surge and fallout deposits that formed the Atexcac axalapazco in the eastern Mexican Volcanic Belt. We defined six different depositional facies based on variations in grain size, composition and depositional structures. The depositional facies defined in this study indicate that the Atexcac axalapazco was formed through phreatomagmatic, phreatic and magmatic explosions. The fluctuations on the availability of groundwater of a local aquifer allowed intermittent interaction with periodic injections of ascending magma bodies and resulted in explosions with different grades of efficiency in fragmentation. In some cases availability of groundwater was almost null, producing only magmatic explosions. The deposition of material of those defined facies was accompanied by ballistic blocks of different compositions (basaltic, limestone, andesitic, microdioritic, juvenile and altered rocks). Velocities of those blocks were modeled, resulting at infrasonic speed (~ 0.3 Mach). The compositions and directions of sampled ballistic blocks allowed us define three different explosive stages with various location zones inside the crater. The evolution of these likely explosive zones suggests a migration and alternation, and sometimes simultaneity of the explosive locus that originated the elongated and irregular morphology of actual crater.

Key words: maar volcanoes, ballistic blocks, eruptive locus migration, depositional facies.

RESUMEN

Explosiones de tipo freático, freatomagmático y magmático produjeron una secuencia estratificada alternada de depósitos de oleada y caída que dieron lugar a la formación del axalapazco Atexcac, en la porción oriental del Cinturón Volcánico Mexicano. Se definieron seis tipos de facies basadas en variaciones del tamaño de grano, la composición y las estructuras deposicionales. Las facies deposicionales definidas en este estudio, indican que el axalapazco Atexcac fue formado a través de explosiones freatomagmáticas, freáticas y magmáticas que ocurrieron en diferentes sitios de explosión. Fluctuaciones en la disponibilidad de agua subterránea de un acuífero local, permitieron la interacción intermitente con inyecciones periódicas de cuerpos de magma ascendentes que resultaron en explosiones con diferentes grados de eficiencia en la fragmentación. En algunos casos, la disponibilidad de agua subterránea fue casi nula, produciendo únicamente explosiones magmáticas. La depositación de material de las facies fue acompañada por bloques balísticos de diferentes composiciones (basáltica, caliza, andesítica, microdiorítica, juvenil y rocas alteradas). Las velocidades a la que fueron expulsados estos bloques resultaron ser infrasónicas (~ 0.3 Mach). Las composiciones y direcciones de los bloques balísticos muestreados permitieron definir al menos tres etapas explosivas que muestran amplias zonas de localización de los focos eruptivos dentro del cráter. La evolución de esas probables zonas explosivas sugieren la migración y alternancia, y en algunas ocasiones, simultaneidad de focos explosivos que originaron la morfología elongada e irregular del cráter actual.

Palabras clave: volcanes maar, bloques balísticos, migración del foco eruptivo, facies deposicionales.

INTRODUCTION

Maars are volcanic craters up to 2-3 km wide (Lorenz, 1973, 2003b, 2007; Jordan *et al.*, 2013) and in some cases up to 5 km (Németh *et al.*, 2001) whose crater floor subsided below the syn-eruptive surface (Self *et al.*, 1980; Wohletz and Sheridan, 1983; Lorenz, 1986, 2003b, 2007; Sohn, 1996), hence pre-maar country rock exposed in their crater walls (Ollier, 1967; Lorenz, 1986, 2003b, 2007; White and Ross, 2011). Maars are commonly filled partially with water of lakes (Carrasco-Núñez *et al.*, 2007), however, they also can be dry. The characteristics deposits forming the surrounding tephra ring are dominated by base surge and fall deposits (Lorenz, 1973; Németh *et al.*, 2001; Wohletz and Sheridan, 1983; White and Ross, 2011; Kereszturi and Németh, 2012), these ejecta beds decrease in thickness very rapidly outward (Lorenz, 1986; Németh *et al.*, 2001). There is a general idea that maars are formed due to explosive magma-water interaction during phreatomagmatic explosions (Fisher and Waters, 1970; Kienle *et al.*, 1980; Lorenz, 1973, 1986, 2003b, 2007; Lorenz *et al.*, 2002; Self *et al.*, 1980; Wohletz, 1986; Németh *et al.*, 2001; Valentine *et al.*, 2011; Kereszturi and Németh, 2012).

In Mexico we use the general term "xalapazco" from the ancient Nahuatl language, meaning vessel containing sand, to name the maar volcanoes; however, when the craters have a lake inside, they are called "axalapazcos", as the prefix "a" means "water".

Therefore an axalapazco is a crater lake that forms in a volcanic crater or caldera, such as a maar. Atexcac, in strict sense, is an axalapazco as it has a beautiful emerald-colored lake inside. The Atexcac axalapazco is located in the central part of the Serdán-Oriental basin in the eastern Mexican Volcanic Belt (Figure 1a and 1b). The Serdán-Oriental basin is dotted with several volcanic structures such as basaltic cinder

López-Rojas, M., Carrasco-Núñez, G., 2015, Depositional facies and migration of the eruptive loci for Atexcac axalapazco (Central Mexico): implications for the morphology of the crater: Revista Mexicana de Ciencias Geológicas, v. 32, núm. 3, p. 377-394.

cones, rhyolitic domes (Riggs and Carrasco-Núñez, 2004; Carrasco-Núñez and Riggs, 2008; Zimmer *et al.*, 2010) and about a dozen of maar volcanoes of either basaltic (Carrasco-Núñez *et al.*, 2007; Ort and Carrasco-Núñez, 2009) or rhyolitic (Austin-Erickson, A., 2007; Austin-Erickson *et al.*, 2008; Zimmer *et al.*, 2010; Austin-Erickson *et al.*, 2011;) composition. The Atexcac axalapazco has an elliptical shape in map view (Figure 1c) with maximum axes between 1,150 and 850 m, being the largest dimension oriented in the ENE direction. Carrasco-Núñez *et al.* (2007) demonstrate that the Atexcac axalapazco was formed as a result of intense phreatomagmatic explosions revealing strong fluctuations in the availability of external water, temporal migration of the locus of explosions and periodic injection of magma.

The general stratigraphic column of Atexcac axalapazco proposed by Carrasco-Núñez *et al.* (2007), includes: 1) pre-maar units, comprising: a) limestone basement rocks of Mesozoic age forming the core of the crater´s western wall (Gasca-Durán, 1981), b) a massive basaltic lava flow outcropping at the lake level, c) a stratified sequence of basaltic scoria (cinder cone) overlying the limestone rocks, d) brown tuff

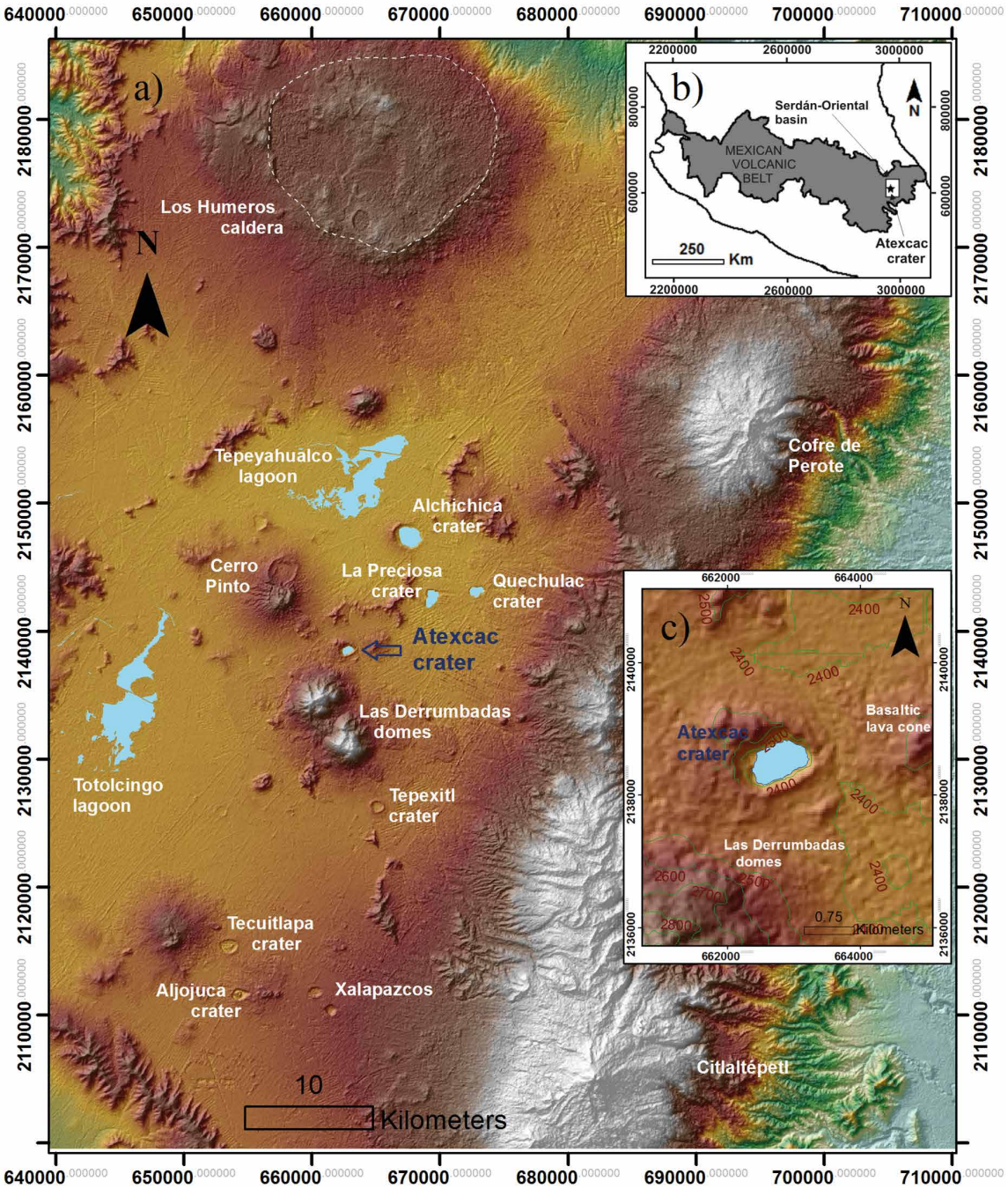

Figure 1. a) Location of the Atexcac axalapazco in Serdán-Oriental basin, showing the main volcanoes at the Citlatépetl-Cofre de Perote range and Serdán-Oriental basin to the west. The Atexcac axalapazco is located in middle part of Serdán-Oriental basin, just southeast of Cerro Pinto ring and dome complex and north of Las Derrumbadas rhyolitic dome complex. b) Location of Serdán-Oriental basin and Atexcac axalapazco in the Eastern Mexican Volcanic Belt. c) Detail of shape of current crater of Atexcac axalapazco with its inner lake.

deposits overlying the basaltic lava flow and e) a rhyolitic pumice-rich tuff deposit, probably correlated with the nearby Cerro Pinto rhyolitic domes and rings complex (Zimmer *et al.*, 2010); 2) the maar sequence, comprising surge and fallout deposits and; 3) post-maar units that consist in a massive obsidian breccia, overlying by an incipient soil. We focus our study on the depositional facies of the maar deposits and the evolution of morphology of the crater assuming lateral variations of the eruptive foci.

The phreatomagmatic explosions may originate large ballistic fragments of the country rock or fresh magma (Self *et al.*, 1980; White and Schmincke, 1999; Németh *et al.*, 2001; Lorenz, 2007; Kereszturi and Németh, 2012; Jordan *et al.*, 2013), which exit to the atmosphere with parabolic-to-hyperbolic trajectories, due to the resistance that offer the air when the fragments are transported through the atmosphere (McGetchin *et al.*, 1974). Bomb sags are good indicators of the source area of the ballistic clasts, however, in many cases, the deposition surface was composed of either coarser grained pyroclastic deposits or it was not wet enough to deform plastically upon impact of ballistic blocks at the Atexcac axalapazco, therefore we consider also some other conditions to infer ballistic trajectories. We only take into account ballistics with elongated shape because ballistic projectiles are ejected from the explosive locus following a general parallel trajectory along its larger diameter, however they may turn around along this axe during transport. Thus, the projectile will remain with its major axis on direction of its trajectory, this is especially true for large blocks, travelling short distances as observed through videos on different volcanoes (Waitt *et al.*, 1995, Taddeucci *et al.*, 2012), thus we consider mostly big elongated lithic (dense) blocks, which are considered to be less affected by modifications of their travel in the air, than small or equidimensional blocks.

We present an inverse study inferring trajectories of large ballistics blocks (from 10 cm to 2 m in diameter) emplaced in different facies and try to explain the lateral migration of explosive locus during the evolution of this maar volcano. The inferences about alternation of different explosive locus are used to explain the morphology of the crater as it can be seen today.

PHYSICS IN THE ATMOSPHERIC TRANSPORT OF BALLISTIC FRAGMENTS

During explosive eruptions volcanoes can eject fragmented material to the atmosphere to velocities, in some cases, at up to hundreds of meters per second (Minakami, 1942; Nairn and Self, 1978; Fagents and Wilson, 1993; Bower and Woods, 1996) and in others cases these velocities may become supersonic (> 1 Mach) in the surrounding atmosphere (Fudali and Melson, 1972; Nairn, 1976). In order to estimate exit velocities, there has been formulated mathematical algorithms that consider the air drag, assuming a constant drag coefficient (Minakami, 1942) or a variable drag coefficient (Wilson, 1972; Waitt *et al.*, 1995; Alatorre-Ibargüengoitia and Delgado-Granados, 2006). In addition, there have been used methodologies based in photo-ballistics (Nairn and Self, 1978; McGetchin *et al.*, 1974; Ishihara, K., 1985) and more recently techniques of remote sensing like Doppler radar (Donnadieu *et al.*, 2005; Gouhier and Donnadieu, 2011) and analysis through high-speed cameras (Taddeucci *et al.*, 2012; Taddeucci *et al.*, 2014).

Experimentally, ejection velocities in explosive molten-fuel-coolant interactions have been obtained by Büttner *et al.* (2002) and Zimanowski *et al.* (1997a) in 100 and 75 m/s, respectively. Self *et al.* (1980) estimated velocities of 100 m/s for large blocks at Ukinrek maars. Ballistic trajectories has been used to explain the morphology of volcanic craters; Pfeiffer (2001) used size distribution of ballistic blocks to estimate vent development during the Minoan eruption of Santorini volcano. More recently, Swanson *et al.* (2012) used ballistics block distribution to infer location of eruptive vents of Kilauea volcano and Jordan *et al.* (2013) used velocities of 100 m/s for modeling ballistic clasts and proposed coalescence of multiple shallow craters to explain the morphology of Purrumbete Lake maar.

The resistance of air changes slightly the trajectory of ballistic clasts when they are transported through the atmosphere, varying from a parabolic to a hyperbolic trajectory (McGetchin *et al.*, 1974). Between forces acting during atmospheric fly of ballistic fragments we can find the velocity of the fragment (V), the drag force (Fd) and the acceleration due to gravity (g) (Sherwood, 1967; Mastin, 2008). Velocity acts along the orientation of the fragment´s trajectory, drag force opposes the motion of the fragment and the gravitational acceleration acts towards the Earth´s centre (Figure 2). At same time, drag forces depend on the dimensionless drag coefficient, which is a function of the fragment´s shape, air density, and the cross section of the fragment and its velocity.

In order to model trajectories of ballistic blocks of the Atexcac axalapazco we used the model Eject! (version 1.4; Mastin, 2008). The equations that govern the atmospheric flight of ballistic blocks are:

$$\frac{dv_x}{dt} = \frac{F_x}{m} = \frac{-v_x \rho_a v A C_d}{2m} \quad (1)$$

$$\frac{dv_z}{dt} = \frac{F_z}{m} = \frac{-v_z \rho_a v A C_d}{2m} - g\,\frac{\rho_r - \rho_a}{\rho_r} \quad (2)$$

Where ρ_a is air density, ρ_r is density of ballistic block, A is cross-sectional area of the block, C_d is the drag coefficient, m is mass of block, g is gravitational acceleration (9.81 m/s^2), v_x and v_z are the block's velocities, horizontal and vertical, F_x and F_z are the drag forces, horizontal and vertical, and t is time. To solve Equations (1) and (2), Eject! uses a fourth-order Runge-Kutta method (Minakami, 1942; Wilson, 1972). This model assumes that the drag force due to resistance to the atmospheric air is proportional to the square of the fragment´s velocity that is transported through this medium (Sherwood, 1967). A very important factor influencing the trajectory of a ballistic fragment and that we used in modeling with Eject!, is the drag coefficient, which is a direct function of its shape and conditions of the fluid medium through which a fragment moves. Mironer (1979) proposed a drag coefficient depending on the shape and type of regime (laminar or turbulent flow). In this study, we follow the criterion to select the drag coefficient proposed by Mironer (1979).

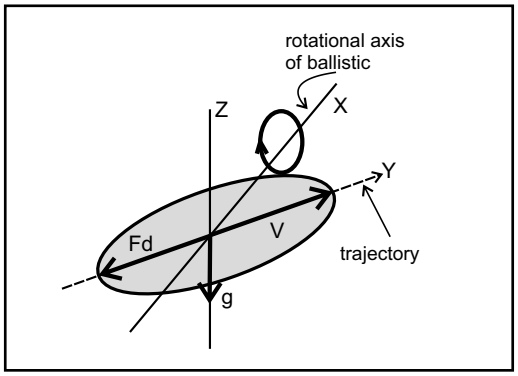

Figure 2. Simple diagram of forces acting during atmospheric transport of a volcanic ballistic. The fragment will follow its path through the "Y" axis while revolving around the "X" axis, driven by a velocity (V), but also breaking forces exerted resistance, which are the force (Fd) of friction (through which fluid moves a fragment) having a direction opposite to the velocity, and gravity (g), directed towards the center of the Earth (adapted of Sherwood, 1967).

DEPOSITIONAL FACIES OF THE ATEXCAC AXALAPAZCO

In order to describe the maar sequence of Atexcac axalapazco two stratigraphic sections were considered: a) a southern section (Figure 3) with the best exposure of facies and better access and, b) a northern section (Figure 4) that served to correlate the occurrence of ballistic fragments during the evolution of Atexcac volcano. To explain the maar sequence we present a description of the six facies defined (see description of facies in Table 1) and the four units containing such facies.

Facies description

The six facies considered in this study are: (1) well-sorted juvenile clasts (Figure 6d), (2) fine ashes, channels and accretionary lapilli (Figure 6c), (3) juvenile clasts with diverse lithics (Figure 6b), (4) breccias and cross-bedded ashes (Figure 7), (5) coarse lapilli layers and massive fine ash, and (6) breccias with megablocks and accretionary lapilli (Figure 7). The main features of these depositional facies are summarized in Table 1.

In general, the facies 4 and 5 are the most abundant in the southern and northern sections; that only show differences on their grain-size distributions. Facies 1 deposits, are only present once, at both southern and northern sections. Facies 2 deposits appear twice in the southern section and only one at the northern section. Facies 3 deposits appear twice at the southern section: the lowermost stratigraphic unit I and the uppermost stratigraphic unit IV occur once at the northern section. Facies 6 deposits are present both at the southern and the northern sections in similar proportions (Figures 3 and 4), but facies of unit I are thinner. In deposits of facies 6 in both sections, occur abundant ballistic blocks of diverse compositions.

Stratigraphic sequence of Atexcac axalapazco

The southern and northern sections were divided into four units following the stratigraphy proposed by Carrasco-Núñez *et al.* (2007) and according to the dominant depositional facies described here for each unit. A brief description of these stratigraphic units is following:

Unit I

Unit I is 10 m thick in the southern section (Figure 3) and only 1 m in the northern section (Figure 4). It is mainly characterized by the marked presence of facies 2. In this unit facies 2 occur at least twice. This same unit contains well-sorted, clast-supported juvenile clasts (facies 1) and facies in the middle part of clast-supported juvenile clasts with diverse lithics (facies 3) which represent pyroclastic fall deposits.

Unit II

Unit II is 30 m thick in the southern section (Figure 3) and 24 m thick in the northern section (Figure 4). It is identified as containing almost only facies 4 and 5. Facies 6 deposits occurs only once, in both sections; and only in the southern section, facies 2 deposits containing ash, sedimentary filled channels and accretionary lapilli structures are present.

Unit III

This unit is 11 m-thick at the southern section (Figure 3) and 23 m-thick at the northern section (Figure 4). In the southern section the facies 4, 5 and 6 are present, and facies 6 is thicker in the northern section. This unit at the northern section is characterized by a very marked dominant presence of 10 m-thick facies 5 deposits which are the thickest facies in both sections (southern and northern).

Unit IV

The upper unit IV is 10 m thick and 13 m in the southern (Figure 3) and northern sections (Figure 4), respectively. There is a difference in facies 3 and facies 6, both with 0.5 m thick, two facies occur in the southern section. In addition to facies 4 deposits, 7m-thick facies 5 deposits appear in northern section.

DISTRIBUTION OF BALLISTIC FRAGMENTS AND SOURCE AREAS

Methodology

During the formation of the maar sequence of the Atexcac axalapazco, explosive water/magma interactions occurred (Carrasco-Núñez *et al.*, 2007), which originated the ejection of a large amount of fragments or blocks, that described atmospheric ballistic trajectories, impacted in the Atexcac stratigraphic sequence, causing bomb sags in some cases. The most suitable configuration to infer trajectories of the ballistic blocks is to use outcrops with vertical exposures whose plane are parallel to the trajectory of the fragment, ideally showing the 3D exposure. We used bomb sags when available, but in other case we use the largest elongated blocks; and in some cases both features when the block remained in situ after landing. In order to have a better accuracy on measurement upon dimensions and to infer the trajectories ballistic blocks, we removed the material that covered each ballistic block, since most of the measured ballistics blocks were embedded on vertical walls of the outcrops. Although the spin of ballistic blocks during its trajectory may be sometimes random or irregular, particularly for equidimensional blocks, we assume that those blocks with elongated shape (an axis dimension greater than the other two axes) are ejected to the atmosphere describing a dominantly rectilinear trajectory (from an aerial view), in which the axis or maximum diameter of the projectile will rotate on a nearly vertical plane (see Figure 2) , but following the straight line, impacting on the ground at a particular angle (that is not necessarily equal to the angle of impact of the projectile trajectory).

In order to infer the atmospheric trajectories we only considered ballistic blocks (Figure 5) with elongated shape that are in situ, with the largest possible size in order to minimize the error possible in the measuring of the trajectories during the airborne travel (Waitt *et al.*, 1995). After checking the in situ stratigraphic position in the field for each projectile, their major, medium and minor diameters were measured using a metric tape; the azimuth was determined using a compass, considering the orientation of the block´s largest diameter and recording the location with a GPS equipment (the UTM coordinates of each ballistic block was measured with an error of ± 3m). This information, recorded in the field for about 43 ballistic fragments (Table 2), was used to integrate a small database in Excel, in which other parameters for each fragment were calculated as the ballistic impact height difference (Figure 8), measured between impact point of ballistic block and crater lake water level. An additional parameter was calculated in this program (Excel), as it is the average ellipsoid for all the fragments (see below calculation method). The dimensionless value of the ellipsoid was calculated by adapting the methodology proposed by Mironer (1979), for which the largest diameter was divided between the average of the middle and lower diameters, for each fragment (Average ellipsoid = maximum diameter/average of middle and minimum diameters). After obtaining the value of the ellipsoid of each fragment, an average of these values was obtained. We obtained an average ellipsoid of around 2, assuming that the fragments moved in a fluid (air) under a laminar flow regime, it corresponds a 0.27 drag coefficient (Mironer, 1979); therefore, for practical purposes a value of 0.3 was used as the drag coefficient. This value was mainly used for the elongated shape of the fragments considered in this study.

To define the likely zones of emission for each ballistic projectile,

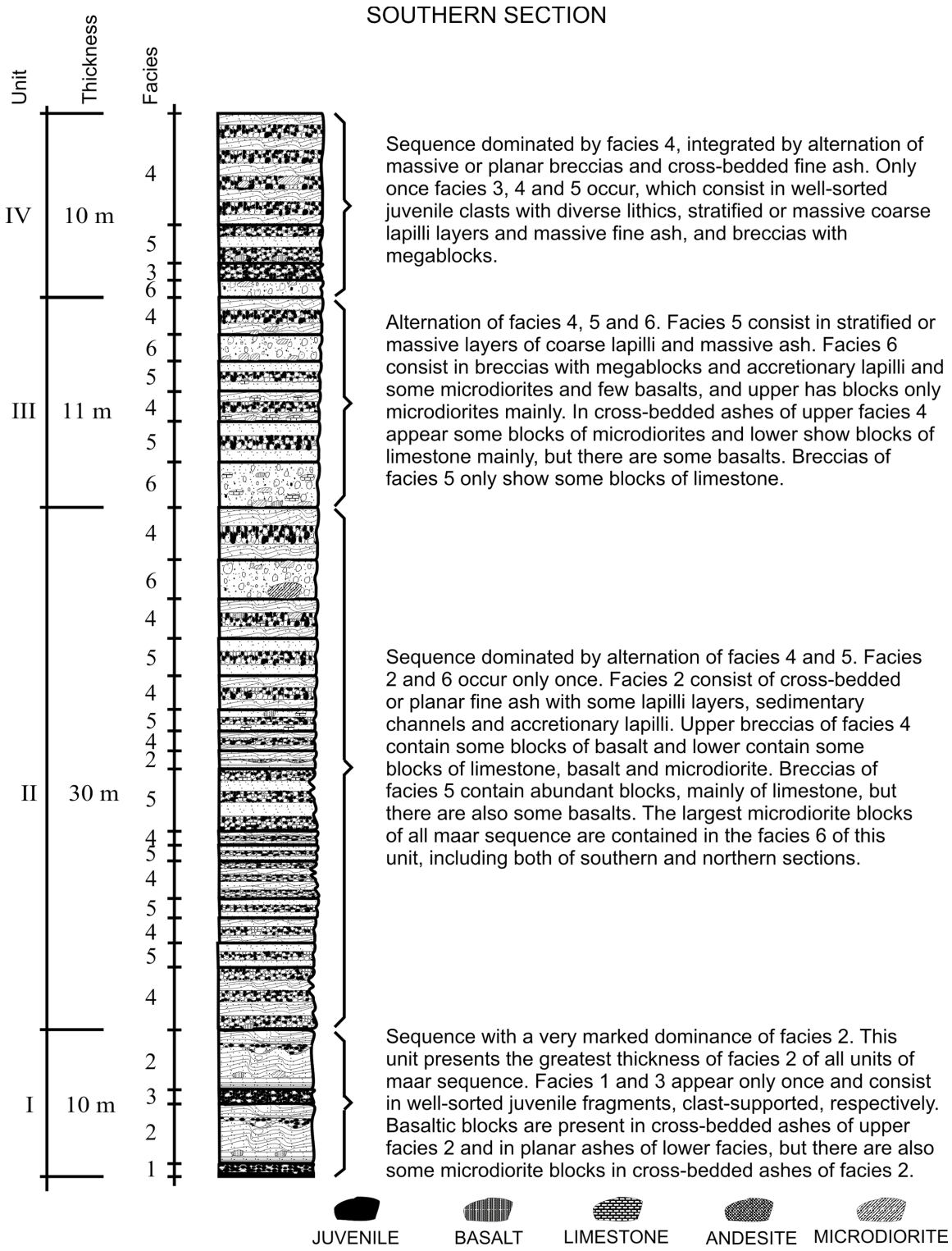

Figure 3. Southern stratigraphic section showing facies considered. Facies 1: Well-sorted juvenile clasts, clasts-supported; facies 2: Fine ashes showing cross-bedded and planar, accompanied by lapilli layers (lithics and juvenile material), some sedimentary filling channels with abundant accretionary lapilli; facies 3: juvenile clasts with lithics, clasts-supported; facies 4: alternation of massive or stratified breccias layers and cross-bedded fine ash; facies 5: alternation of massive or stratified coarse lapilli layers and massive fine ash layers; and facies 6: breccias with megablocks in breccias or ashes with accretionary lapilli. See location of this section in figure 9.

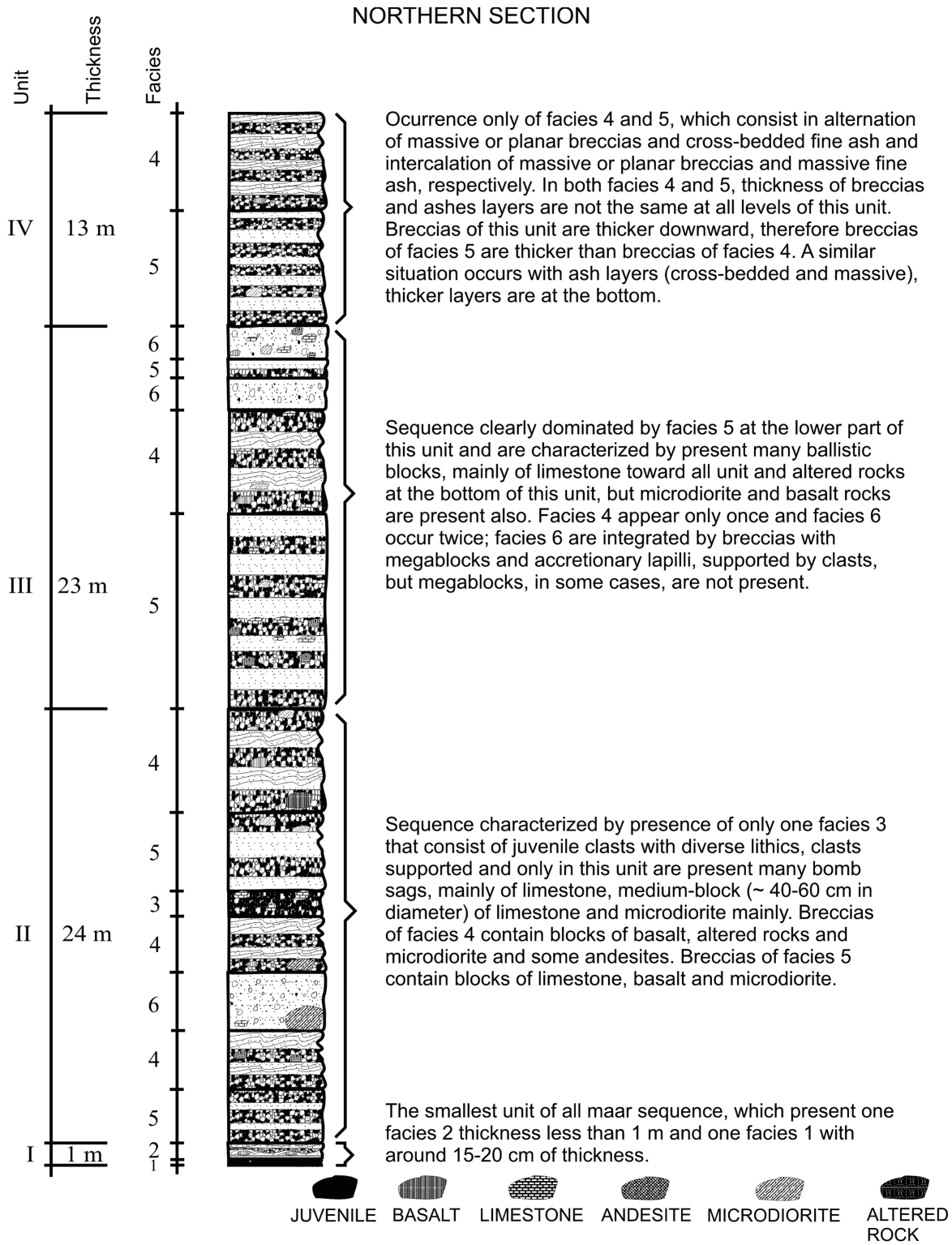

Figure 4. Northern stratigraphic section that shows the different facies forming this section. Notice the difference in thickness, as compared with southern section, particularly of units, mainly, the units 1, 2 and 3. Facies 1 of this unit is the thinnest horizon of all maar sequence. Facies 3 only ocurr once. This section is dominated by facies 4 and 5, although in the unit 1 is not present. In general, ballistic blocks ocurred in breccias in all types of facies at the northern section. See location of this section in figure 9.

Table 1. Description of depositional facies of the Atexcac axalapazco.

Facies	Description
1. Well-sorted juvenile clasts	This facies occurs in the southern column with a thickness of 20 cm and 10-15 cm in the northern section. This includes a lithic-rich, laminated layer (~ 1 mm) of gray color of very fine lapilli followed by a horizon characterized by the dominance of fine lapilli (~ 1 cm diameter) of light gray material mainly juvenile, well-sorted, clasts supported with subrounded shapes, accompanied by a minor proportions of basalt and altered rock lithics with angular shapes and red scoria with rounded shapes (see photographs of Figure 6a and 6d).
2. Fine ashes, channels and accretionary lapilli	Consist dominantly of fine gray ash layers with planar and/or cross-bedded structure, with some layers of lapilli, presence of sedimentary filling channels and accretionary lapilli (Figures 6A and 6C). Fine ash layers contain angular lithic fragments of basalt and limestone with scarce juvenile material. Filling channels consist of poorly-sorted massive breccias (of fine to medium lapilli) of juvenile material and diverse angular lithic, without apparent gradation. Both stratified ashes and filling channels, show bomb sags produced by ballistic blocks of andesite, basalt, limestone and microdioritic (Yáñez and García, 1982) rocks, which caused some degree of plastic deformation, especially on the fine ashes. There is a clear dominance of fine-grained layers of planar and cross-bedded ashes (see photographs of Figure 6a and 6c).
3. Juvenile clasts with diverse lithics	These facies are characterized by massive breccias supported mostly by clasts, scarce presence of fine to coarse ash matrix, containing juvenile fragments ranging in size from fine lapilli to block, with dominance between juvenile material coarse lapilli-sized (Figure 5a and 5b). Juvenile clasts are complemented with a lower proportion of angular lithic basalt, limestone and altered rocks. In some cases, the grain-size of juvenile material and lithics, ranging from very fine lapilli to small blocks and other grain-size is fine lapilli (see photographs of Figure 6a and 6b).
4. Breccias and cross-bedded ashes	Facies 4 deposits consist of an alternation of massive or planar breccias and cross-bedded fine ash. Stratified ash horizons have limited presence of lithic lapilli-sized, mostly limestone and very little content of basalts, altered rocks, scoria and juvenile fragments. Some bomb sags of ballistic blocks are presented in both the breccias and ash horizons. The breccia layers are moderately sorted and show massive structure or diffuse planar stratification of lithic and juvenile fragments, with a dominance of lithics fragments of basalt and altered rocks, and very few microdioritic and scoriae clasts. The proportion of lithic fragments and juvenile clasts in the breccias is about 80-20% (by component analysis). See photography of Figure 7.
5. Coarse lapilli layers and massive fine ash	It includes stratified and massive coarse lapilli and massive ash. These stratified layers are breccias composed of altered lithics, basalts, microdioritic and limestone rocks with very little presence of juvenile fragments. Although the breccias are supported by clasts, there is a very incipient presence of ash matrix, which is intercalated with some very thin layers (~ 3 cm) of cross-bedded fine ash. These ash layers have, in most cases a massive structure, but in some places they have a very diffuse planar stratification. Also a few lithic basalts and juvenile very fine lapilli, but in some levels, it can be seen fine lapilli clasts of altered rocks and limestone.
6. Breccias with megablocks and accretionary lapilli	The breccia deposits have a very marked difference compared to breccias of facies 4 and 5, the clasts are supported basically, composed of by a more than 2 m-thick breccias with fragments of fine to coarse lapilli of limestone and juvenile clasts. There are some small and medium-sized limestone blocks and microdioritic clasts and a few basalt clasts. In some levels, these breccias have a diffuse planar structure, but in general is massive and chaotic. The shapes of lithic lapilli fragments, as well as the blocks, range from subangular to angular (see photography of Figure 7).

modeling was performed through the Eject computer program, version 1.4, developed by Mastin (2008). The input data used for the modeling for each projectile launched were: a drag coefficient of 0.3 (for all modeling), the density of the projectile according to the type of rock that is composed (basalt, andesite, microdioritic, limestone, etc; see Tables 2 and 3), the diameter of the projectile (obtained as the average diameter of the larger diameter, medium and low), the ballistic emission angle, ejection velocity and the ballistic impact height difference. Alternately the Eject and Excel programs were used to determine, in each modeling, the farthest point of where likely come from each ballistic, using an angle of 45° (Figure 8); of the same way the closest point was obtained of which could be from the same ballistic, considering emission angle of about 85°. Then the midpoint between these two points was determined and defined two zones along the line trajectory of the fragment; a more proximal likely zone of ballistic ejection, between the middle point and the emission point considering the angle of 85 ° (Figure 8), that is, we estimate a maximum and minimum travel distance that suggest a likely range regardless the variation of the ejection angle. Judging by the stratigraphic position at the subsurface inferred by Carrasco-Núñez *et al.* (2007) from the different lithologies identified in the maar-forming stratigraphic columns, we consider that a zone is more likely for the ejection of limestone, andesite, microdiorites and juvenile blocks, inferring that ballistic blocks with these compositions may come from zones that are not exposed and underlie the basaltic rocks that are exposed at the bottom of the crater at the level of the lake. However, these lithologies that form the underground country rock doesn´t have to be too deep, we can estimate a few hundreds meters but less than 1 km. Therefore, it may be possible that those blocks come from relatively shallow depths and/or some might come from even shallower near-surface explosions, as a result of vertical mixing of material derived by upward-directed debris jests and downward collapse, as proposed by Valentine and White (2012). It may be likely that the ejection of basalts that are exposed just at the level of the crater, may result from direct ejection.

Ballistics distribution maps with facies sections

In order to have a general and rough estimation of the source of the ballistic blocks originated during phreatomagmatic explosions, it is important to have a general stratigraphy of the country rock, underneath the Atexcac axalapazco, even if we consider that the blocks travel directly from the source or, more likely, they mix during the vertical travel to the surface to finally erupt from shallower levels (Valentine and White, 2012). In addition to the rocks exposed on the Atexcac crater´s walls (basalts), other non-exposed rock units such as limestone, andesite and microdioritic rocks has been inferred to exist at relatively shallow locations underneath the volcano based on the abundance of these clasts in the maar-forming deposits (Carrasco-Núñez *et al.*, 2007). Even though some clasts may be recycled during multiple explosions (Ross and White, 2006; Valentine *et al.*, 2011; White and Ross, *2011).*

Ballistic fragments were distributed during the formation the maar sequence through all deposits. In fact, there are very abundant in facies of the four stratigraphic units of Atexcac crater maar sequence,

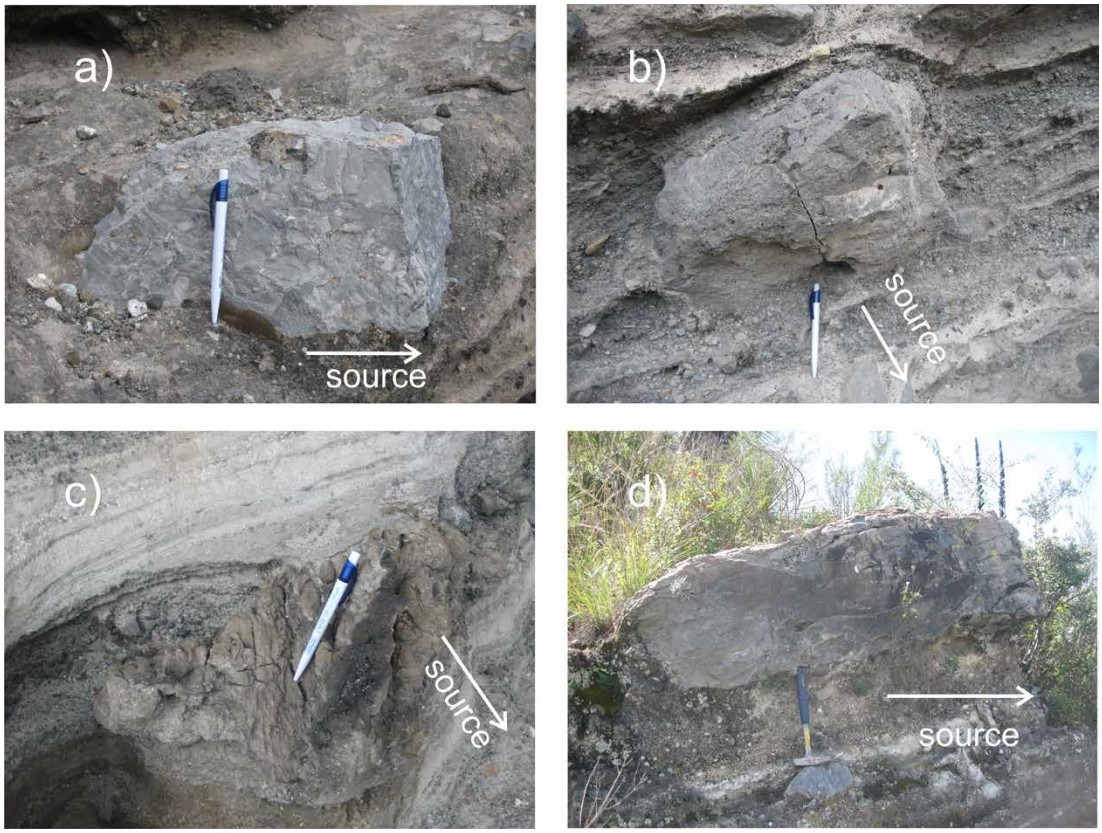

Figure 5. Photographs showing four different types of ballistic blocks: a) limestone block (A35), maximum diameter 33 cm, impacted on cross-bedded ashes at facies 4; b) basalt block (A36), maximum diameter 45 cm, impacted on massive at ash facies 5; c) juvenile block (A43) with bread crust, maximum diameter 20 cm, impacted on cross-bedded ashes at facies 4 and; d) one of the largest microdioritic blocks (A23) with a maximum diameter of 2.3 m, impacted on breccia at facies 6. A35, A36 and A43 blocks were impacted at the northwestern wall of crater; A23 block impacted at southern wall of crater. Size of pen in photographs a), b) and c) is 15 cm. Size of hammer of photograph d) is 33 cm.

but it was only possible to take into account 43 large fragments with elongated shape and that satisfy the requirements mentioned above. Units I, II and IV contain the ballistics measured in this work (Table 2).

Ballistic blocks of stratigraphic units I and II were measured in the southern wall of crater and of unit IV were measured in the northeast and northwest walls (Figure 9). Most of the ballistics were measured in the southern wall of the inner crater because there is a better access. The biggest ballistic blocks (> 2 m) measured are microdioritic clasts but the most abundant are limestone blocks.

The explosions that originated the deposits during the formation of stratigraphic unit I, produced ballistic blocks, mainly of basaltic composition, but microdiorite, limestone and andesite are also present. It is very likely that explosions that produced the first deposits and the ballistic blocks of the lower part of unit I formed a protodiatreme (Valentine and White, 2012) in the initial stages upon formation of Atexcac axalapazco.

Unit II is characterized for the dominant presence of limestone blocks with a lower amount of limestone and basalt blocks and some andesite. Unit III has a very marked dominance of limestone blocks, some microdiorites and few basalt and altered rock blocks.

Facies 2 deposits show structures with the greatest plastic deformation caused by ballistic impacts (taking into account ballistic diameters and deformation of underlying layers), but also lesser amount of bomb sags; this is associated to more efficient fragmentation due to better ratio water/magma (Carrasco-Núñez *et al.*, 2007) or to the lower energy available for ejecting ballistic blocks and the resulting product of the phreatomagmatic explosions was deposited in wetter conditions. The deformation caused by ballistic impacts, in some cases, is almost the same to the block´s diameter or alternatively some underlying layers can be broken by the ballistic impact, possibly due to the high density of the blocks.

In the case of unit I (Figure 10), the explosions apparently occurred simultaneously in different areas inside the crater, although preferentially from the western and central zones. Most of the blocks are basaltic clasts suggesting sub-surface explosions; however the presence of lower microdioritic blocks may be linked to occurrence of some relatively deeper explosions but at a depth where hydrostatic pressure in the aquifer is less than the critical pressure (Valentine and White, 2012).

During the emplacement of the stratigraphic unit II, ballistic blocks came mainly from the southern and southwest zones of the crater, but also there were some ballistic blocks coming from the northern and northwest parts (Figure 11). This unit has more ballistic blocks compared with previous units and the more abundant compositions are microdioritic and limestone clasts. This could suggest a change in the original strength of the country rock that produced more ballistic blocks (Valentine *et al.*, 2015) of explosive events that originated most of the facies of this unit comparing with the previous unit, without taking into account, cross-bedded ashes contained in facies 4. Even so, cross-bedded ashes of facies 4 appear to be deposited under less wet conditions compared with cross-bedded ashes of facies 2 (in facies 2 appear accretionary lapilli). The larger microdioritic blocks occurred

Table 2 . Location and characteristics of ballistics measured and considered in this study.

Number	UTM coordinates		Composition	Average diameter (cm)	Ellipsoid	Density (kg/m³)	Az (degrees)	Impact heigth difference (m)	Ejection velocity (m/s)
	X	Y							
A01	662,581	2'138,119	Basalt	19.33	1.87	2,900	316	58	100
A02	662,582	2'138,117	Basalt	17.33	1.71	2,900	311	56	100
A03	662,587	2'138,119	Andesite	21.67	1.71	2,400	345	56	110
A04	662,605	2'138,133	Basalt	15.67	2.09	2,900	348	54	100
A05	662,613	2'138,129	Basalt	13.67	1.73	2,900	354	66	105
A06	662,613	2'138,129	Microdiorite	18.33	2.40	2,800	36	62	100
A07	662,620	2'138,128	Basalt	23.00	1.73	2,900	45	57	100
A08	662,625	2'138,119	Microdiorite	20.00	1.75	2,800	298	58	100
A09	662,634	2'138,138	Microdiorite	15.00	2.09	2,800	46	57	100
A10	662,663	2'138,137	Limestone	12.33	1.89	2,400	309	57	100
A11	662,673	2'138,138	Basalt	20.00	1.75	2,900	29	59	100
A12	662,682	2'138,144	Basalt	16.67	1.70	2,900	292	60	100
A13	662,685	2'138,147	Microdiorite	14.33	1.74	2,800	342	60	100
A14	662,689	2'138,145	Limestone	21.67	1.94	2,400	300	61	100
A15	662,703	2'138,147	Microdiorite	30.33	1.71	2,800	338	61	100
A16	662,713	2'138,144	Limestone	11.00	1.67	2,400	30	67	100
A17	662,732	2'138,156	Microdiorite	19.00	1.93	2,800	339	72	100
A18	662743	2'138,161	Basalt	10.33	1.88	2,900	329	72	100
A19	662,769	2'138,162	Microdiorite	54.33	2.18	2,800	327	82	100
A20	662,777	2'138,157	Limestone	25.67	2.16	2,400	3	93	100
A21	662,778	2'138,156	Microdiorite	26.67	2.00	2,800	355	94	100
A22	662,782	2'138,154	Basalt	32.00	1.56	2,900	38	94	100
A23	662,777	2'138,147	Microdiorite	136.67	2.56	2,800	329	91	100
A24	662,814	2'138,144	Andesite	15.00	1.75	2,400	14	93	100
A25	662,803	2'138,138	Limestone	30.67	1.91	2,400	330	94	100
A26	662,847	2'138,145	Andesite	31.67	2.75	2,400	319	101	100
A27	662,904	2'138,118	Microdiorite	15.00	2.50	2,800	356	104	100
A28	662,905	2'138,119	Limestone	33.33	2.00	2,400	302	103	100
A29	662,895	2'138,129	Microdiorite	23.00	1.73	2,800	319	104	100
A30	662,897	2'138,126	Andesite	25.33	1.71	2,400	18	105	100
A31	662,902	2'138,124	Limestone	18.00	1.48	2,400	323	107	100
A32	662,154	2'138,776	Basalt	30.00	1.60	2,900	106	115	110
A33	662,155	2'138,768	Juvenile	21.67	1.71	1,400	103	176	120
A34	662,158	2'138,744	Basalt	35.67	1.75	2,900	120	168	100
A35	662,155	2'138,751	Limestone	20.67	2.28	2,400	94	173	120
A36	662,104	2'138,760	Basalt	37.67	1.32	2,900	142	165	100
A37	662,099	2'138,750	Andesite	26.00	1.39	2,400	111	162	120
A38	663,160	2'138,921	Microdiorite	19.67	1.37	2,800	189	126	100
A39	663,142	2'138,938	Microdiorite	16.67	1.45	2,800	218	130	100
A40	663,157	2'138,926	Microdiorite	27.00	1.95	2,800	198	135	100
A41	663,189	2'138,908	Basalt	13.67	1.42	2,900	253	121	120
A42	663,190	2'138,911	Microdiorite	16.33	2.67	2,800	242	118	100
A43	663,187	2'138,913	Juvenile	14.33	1.74	1,400	231	117	120

in stratigraphic unit II (> 2 m of diameter) and appear in the facies 6 of unit upper part.

The intercalated occurrence of microdioritic blocks, during formation of unit II, with the other types of blocks (basalt, limestone and andesite), suggest that it is likely that there was a previous vertical mixing of clasts that finally were erupted by explosions more shallow (Valentine *et al.*, 2014). In addition, may have alternation of explosive locus in location and perhaps depth; of which, basalt come from sub-surface zones and andesite and limestone from an apparently shallow zone. In general, basalt and limestone blocks were ejected during explosions that formed breccias in facies 4 and 5, and microdioritic blocks of the lower and middle part of unit II occurred through explosions that caused cross-bedded ashes. This may be associated to a more mature stage of the diatreme growth (Valentine and White, 2012, 2012; Valentine *et al.*, 2014) whose explosions fragmented fresh magma of feeder dike and subrounded country rock. The microdioritic blocks ejected at the upper part of unit II were originated during the formation of one of the facies 6 deposits, integrated by a great amount of blocks with diverse size. In the same way of cross-bedded ashes of facies 2 of the unit I, ashes of facies 4 deposits show the greatest deformation by ballistic impacts. In some cases, this deformation is bigger than the diameter of ballistic fragment, but deformation is smaller than that showed by cross-bedded ashes layers, suggesting that these layers were formed in wetter conditions.

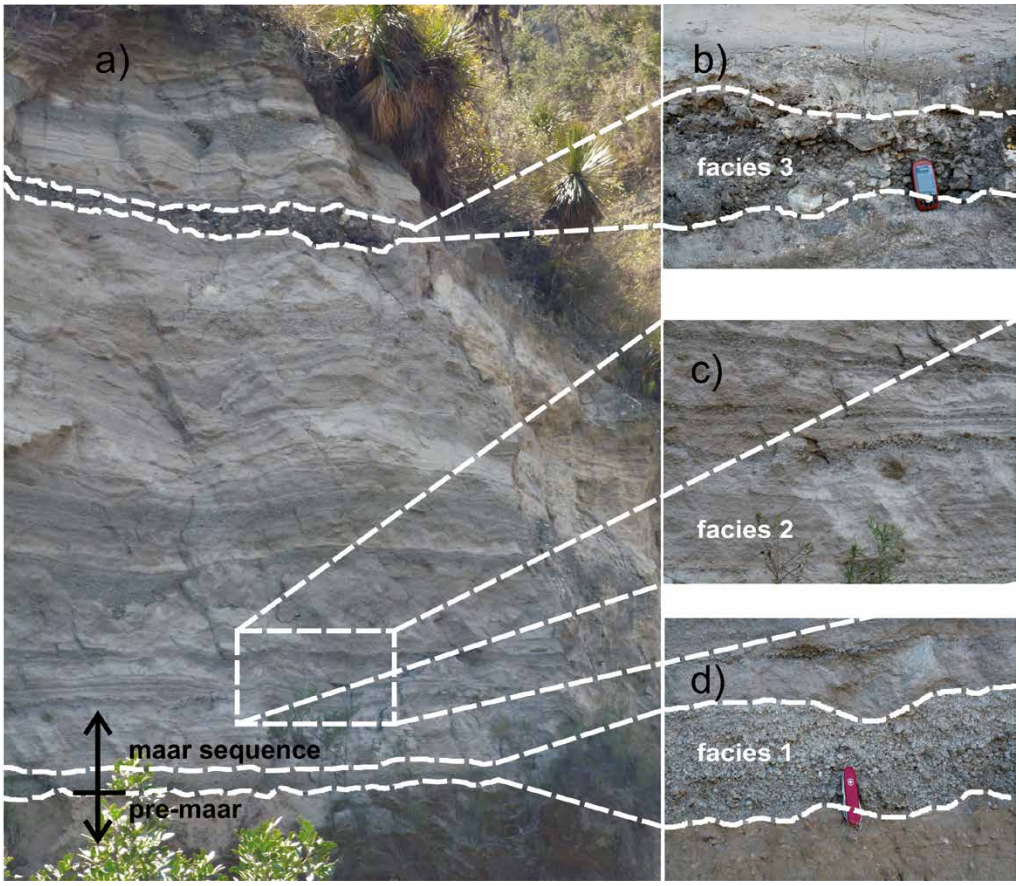

Figure 6. Photographs showing different facies: a) Facies 1, 2 and, 3, and brown tuff (toba café), a layer of pre-maar sequence. b) Detail of facies 3 of photo a), showing a massive breccia, clasts-supported, consisting of juvenile material and diverse lithics. The size of red color GPS is 10 cm. c) Detail of rectangle of the bottom of facies 2 of photo a), showing cross-bedded and planar layers and sedimentary filling channels; at the bottom it is showed part of facies 1. The dimensions of rectangle are 1.0 × 1.8 m. d) Detail of facies 1 of photo a), showing a juvenile scoria fallout material, the upper part is the facies 2 and the lower part is brown tuff of photo (a). The size of knife is 10 cm. The maar sequence started with facies 1 and the contact with pre-maar units is showed in photo (d).

Figure 7. Photography showing facies 4 and 6. The upper image show intercalations of massive or planar breccias and cross-bedded fine ash corresponding to facies 4. We can see a little bomb sag produced by an ballistic block of limestone. At the bottom of image it shown just a part of facies 6, but they can be seen lithic lapilli fragments of different lithologies. The size of hammer is 33 cm.

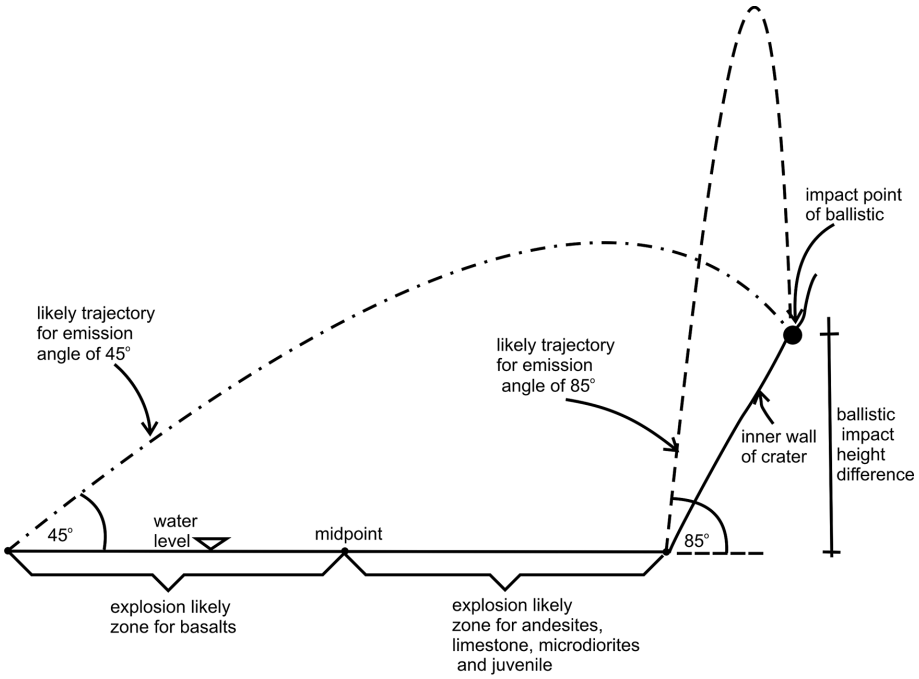

Figure 8. Schematic diagram showing two ejection likely zones of a ballistic considering its composition and according to the ejection angles of 45 and 85 degrees, respectively. It is assumed that the fragments of basalt come from a closer zone to the surface and were apparently ejected from source with a lower angle of emission (45°); while for the case of fragments of andesite, limestone, microdiorite and juvenile, it is inferred that come from a shallow zone and therefore with a higher emission angle (85°).

It was no possible to measure ballistic blocks at unit III in both sections because we found not examples that meet conditions mentioned in the methodology described before for this work, that is, the blocks found have not elongated shapes that serve to infer the trajectory and source area. Ballistics generated during deposition of layers that comprise unit III are very abundant along this unit. Most of them impacted in facies 4 and mainly in facies 6 deposits. Facies 6 of this unit have the highest abundance of microdioritic blocks at the top; while lower facies 6 deposits have abundant limestone and some basalt and microdioritic blocks. Facies 5 of the middle part of this unit have less limestone blocks.

The ballistic blocks measured in the unit IV represent, in this study, the clearest example to determinate that there were alternated and simultaneous explosions that generated fallout and surges deposits of the maar-forming sequence of the Atexcac axalapazco (Figure 12). The presence of accretionary lapilli and the fine grained juvenile material and lithics in facies 3, 4, 5 and 6, within this unit, in both sections, respectively, comparing with unit III, indicate wetter conditions and a more efficient fragmentation. These blocks were mainly basalt and microdioritic fragments, with minor limestones and less andesites. An important feature that characterizes the uppermost part of this unit is the presence of juvenile cauliflower bombs that are present all around at the upper layers of crater, intercalated with accretionary lapilli, suggesting these bombs suffered on its exterior water-chilled (Fisher and Schmincke, 1984; Rosseel *et al.*, 2006) and/or vulcanian explosions occurred (Fisher and Schmincke, 1984).

DISCUSSION

Eruptive stages definition

In order to group the ballistic blocks that occurred during the different explosions that formed the maar sequence of Atexcac, we consider the lines of likely explosion for each ballistic block as configured in figures 10, 11 and 12. With this information we try to define explosion zones, delimited by circles, which were defined after grouping several likely neighbor explosion zones, cut relationships of the crater morphology and stratigraphic level of each ballistic clast. Table 3 shows the ballistic blocks corresponding to each explosive stage and the resulting morphology after each explosive stage, as shown in figure 13. The diameter of each explosion zone (circles) is big enough to absorb possible measurement errors in the field of the ballistic orientation.

Facies interpretation and explosive locus evolution

Eruptive stage 1

The basal, incipient (~ 3cm-thick), lithic laminated layer of facies 1 indicates that the eruption initiated with a preathic eruption (Carrasco-Núñez *et al.*, 2007); which was followed by an ephemeral eruptive column, followed by explosive pulses accompanied by low amounts of lithics of underlying rocks of basalt, limestone and a preexist cinder cone at the beginning of the maar-forming sequence. It is very likely that at this stratigraphic level explosions occurred principally at the southwest sector of the crater and at the boundary of basalts and andesites or very shallow as confirmed by directions and dominantly basaltic composition of ballistic blocks (A1, A2 and A4) at the lowest facies 2 of unit I. At this time, a basaltic magma injection occurred and caused phreatomagmatic explosive events when this magma interacted with water of local aquifer, causing the deposition of cross-bedded and planar, fine to very fine ashes intercalated with the occurrence of small eruptive columns, which caused filled channels originated by surges.

The first basaltic ballistic blocks of the explosive stage 1 (A1, A2 and A4) suggest two alternate and sub-surface explosive locus acting at the southwest and northwest zones, producing surge layers of the lowest facies 2 of unit I. The lapilli-size and minor blocks of the juvenile-rich material of facies 3 together with the orientation of a microdioritic ballistic block show likely magmatic explosive pulses that occurred at the southern sector of crater, at relatively deeper levels that previous events, either as direct ejecta or as stepwise ascent to the surface. A new injection of basaltic magma generated explosive interactions with water of local aquifer producing coarser-grained surge layers of the upper

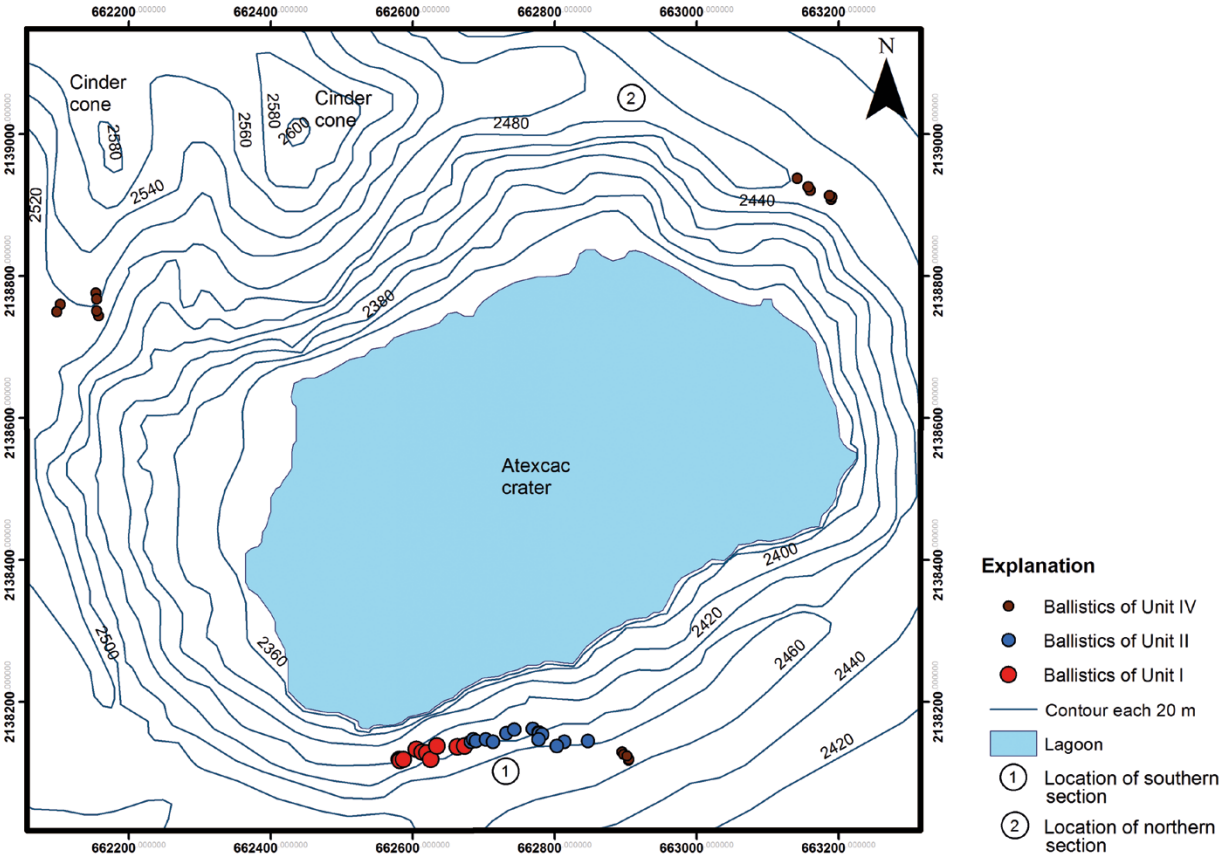

Figure 9. Map of the distribution of ballistic fragments measured in this study. On units I and II only in the southern section ballistics were measured. It was possible to measure ballistic fragments in the stratigraphic unit IV in the NE and SW sectors of the inner walls of the crater, but it was no possible to measure ballistics in unit III. The size of circles doesn´t represent the size of ballistic blocks, only represents ballistic blocks of different stratigraphic units.

facies of unit I, compared with lowest facies 2, and may be associated with changes in the original strength of country rocks underlying (Valentine *et al.*, 2015). The orientation and basaltic composition of ballistic blocks (A5 and A7) indicate, that explosions were shallow and occurred in a fractured aquifer that allowed that explosions with less efficient fragmentation and presumably magmatic, deposited material that filled channels of the lowest facies 2 of unit I, and that explosions occurred at different epicenters at southwest and southern sectors of the crater as suggested by orientation of the limestone (A10) and microdioritic (A8 and A9) ballistic blocks. At the end of the lowest facies 2 of unit I, explosions that deposited surges layers could have migrated towards the crater's center, as suggested by the orientation of basaltic ballistic blocks (A11). The greater thicknesses deposits that forming the unit I at the southern sector of crater, compared those the northern sector, could suggest that surges originated during the emplacement of facies 2, were preferentially originated from southwestern area. After these explosive events, the crater´s morphology changes its shape as shown in figure 13.

Explosive stage 2

After the first explosions of unit I, dominated by surges deposits, the eruption covered a larger region almost in the same site of all previous explosions (stage 1), but extended to the northeast, as shown by breccias and cross-bedded layers of the lower facies 4 at the basal part of unit II.

The alternation of these layers and the diverse composition of the ballistic blocks (basaltic, limestone and microdioritic rocks) in facies 4 may indicate that explosions in the explosive stage 2 occurred at different depths and that there was intermittent availability of water that produced cross-bedded layers (with accretionary lapilli) intercalated with fallout breccias. However, it can also be associated to the occurrence of intra-diatreme explosions, at various levels, whose products were finally ejected through explosions derived from near-surface explosions (Valentine and White, 2012). These breccias could be associated with events when water of the local aquifer was not abundant or was not sufficient to induce explosive interactions with an ascendant magma body. The explosive events of stage 2 were not present at the northern section perhaps due to the closeness to the source. When surges and fallout finished, the eruption evolved to a more magmatic behavior, shown by alternated layers of coarse lapilli breccias and juvenile ash fallout layers. At this stratigraphic level, the explosive locus migrated to the crater´s southeast sector and explosion locus could have been at different levels (Ross and White, 2006; Valentine *et al.*, 2011; White and Ross, 2011) and these explosions produced the first facies 5 of unit II bottom at the crater´s northern sector. The eruption continued with same intermittent behavior that is an alternation of explosive locus localized at the northern, southern and northwest of the crater. This stage 2 includes facies 4 and 5 at the southern sector with different thicknesses and the presence of microdioritic, basaltic and limestone blocks, could means that explosions occurred to different depths with intermittent availability of groundwater without producing long-lasting explosive interactions. In this same stage 2, the explosions caused the deposit of the first breccia characterized by containing larger microdioritic blocks (facies 6) at northern sector that

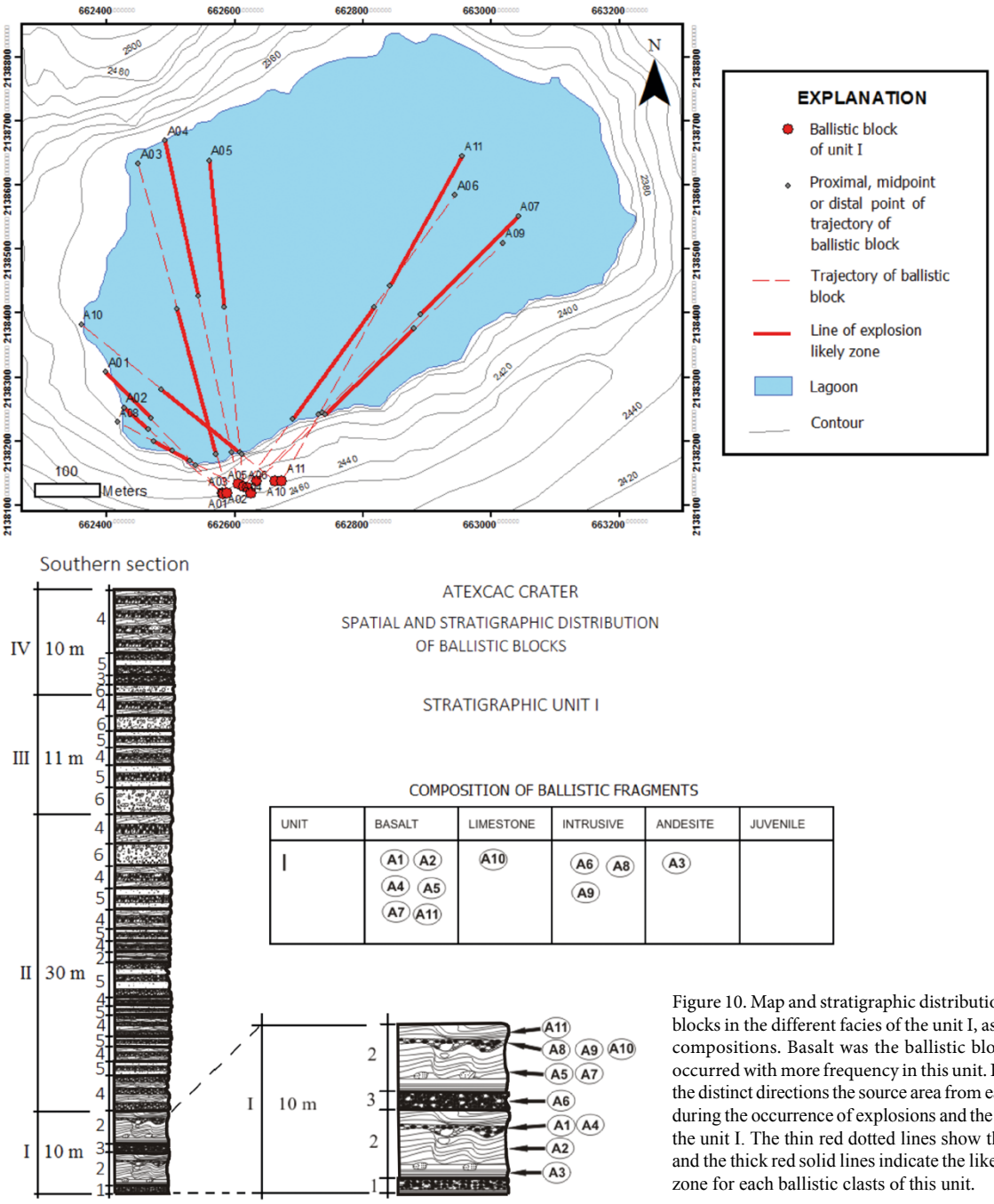

Figure 10. Map and stratigraphic distribution of ballistic blocks in the different facies of the unit I, as well as their compositions. Basalt was the ballistic block type that occurred with more frequency in this unit. It can be seen the distinct directions the source area from each fragment during the occurrence of explosions and the formation of the unit I. The thin red dotted lines show the directions and the thick red solid lines indicate the likely explosion zone for each ballistic clasts of this unit.

indicate lower fragmentation and fracturing of the aquifer country rock. After the rhythmic alternation of facies 4 and 5 of the lower-middle part of unit II a new injection of basaltic magma interacted with the aquifer producing thin cross-bedded and planar layers (facies 2). The intermittent phreatomagmatic behavior of the explosions continued during this stage 2 producing interbedded deposits of thick breccias coarse lapilli with cross-bedded layers (facies 4) and thick coarse breccias with ash fine fallout (facies 5) at the southern and northern sectors. The morphology acquired by the Atexcac crater after these explosions it showed in Figure 13.

We have no data of ballistic projectiles of unit III, neither the southern or northern sectors, but differences between existent facies on type and thickness, indicate some explosions were closer to the southern zone. The presence of breccias with megablocks (facies 6) at both sectors intercalated with ash layers with accretionary lapilli and juvenile ash, suggests explosive phases alternated with phreatomagmatic and magmatic events. These explosive events may have fractured the aquifer allowing subsequent intermittent interaction of magma bodies with groundwater and then generating later, either breccias with cross-bedded layers (facies 4) or breccias with massive ash (facies 5) perhaps associated to opening of a news explosive source. Also, these events could have produced abundant ballistic blocks of facies 6, mainly of basaltic, limestone and microdioritic composition. For example, the greater thickness of facies 4 and 5 of lower and the middle parts of unit III at northern section could suggest a closer explosive source.

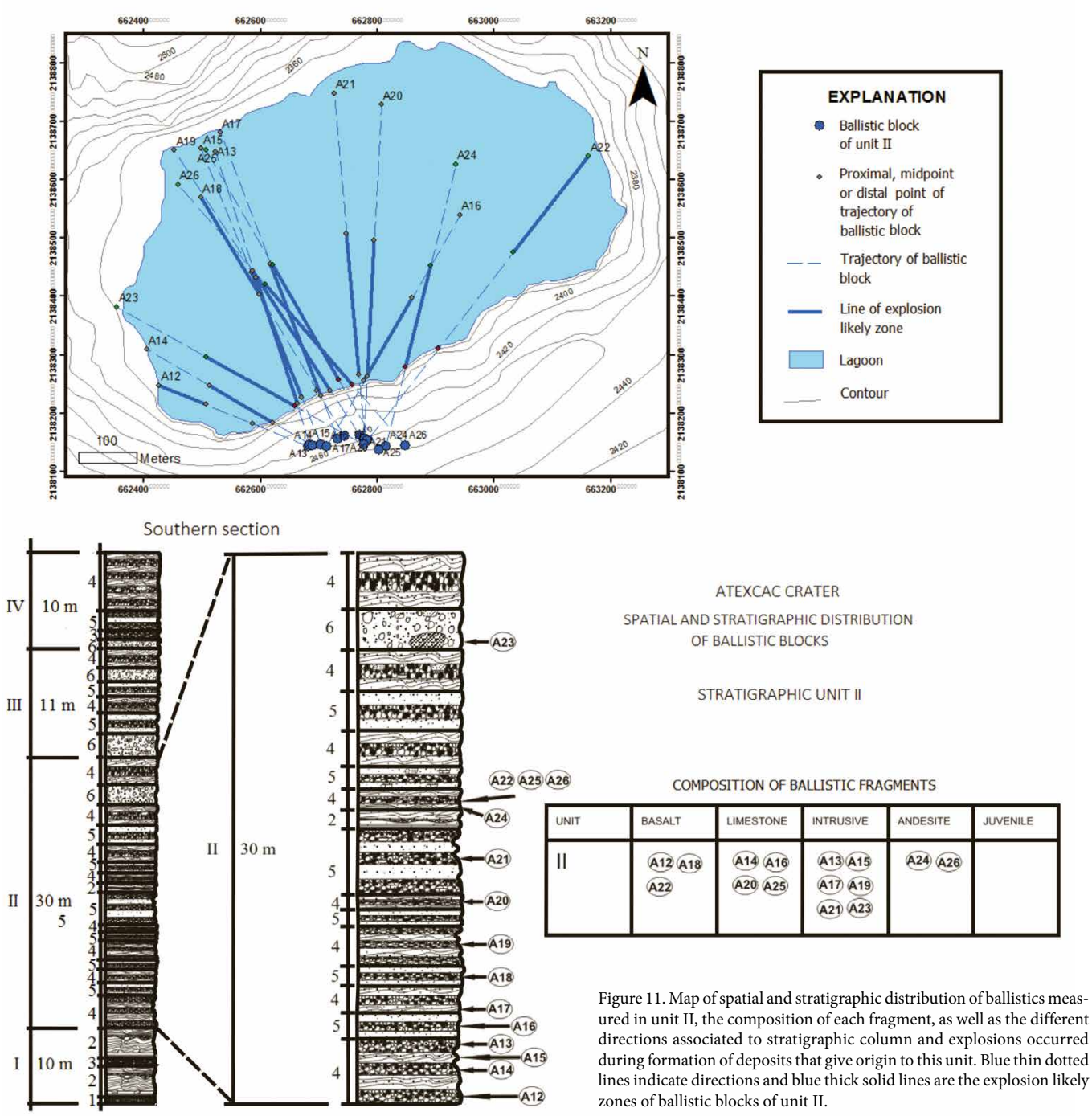

Figure 11. Map of spatial and stratigraphic distribution of ballistics measured in unit II, the composition of each fragment, as well as the different directions associated to stratigraphic column and explosions occurred during formation of deposits that give origin to this unit. Blue thin dotted lines indicate directions and blue thick solid lines are the explosion likely zones of ballistic blocks of unit II.

Eruptive stage 3

The last explosive stage of the maar sequence included depositional facies 6 at the southern sector of crater with impacts caused mainly by microdioritic ballistic blocks, which suggest the occurrence of shallow phreatomagmatic events originated from microdiorite dikes that intruded into limestone rock, which were pushed gradually into higher positions in the conduit-crater system as a result of vertical mixtures of debris jets and downward deposition of eruptive materials (Valentine and White, 2012; Valentine *et al.*, 2014; Valentine *et al.*, 2015). The eruption continued with a magmatic event characterized by the deposition of a massive breccia of juvenile material (facies 3). The source of this event may have been closer of southern sector as indicated by the presence of this layer only at the southern section. The explosions continued through various explosive foci, mainly located at the southern, northern and northeast sectors of the crater and produced interbedded layers of coarse lapilli breccias with massive ash (facies 5). This last facies 5 has a greater thickness at the northern sector and may be occurred closer to the explosive locus to this sector, as indicated by the directions and likely explosive zones of stage 3. These different explosive pulses generated abundant andesitic (A30), basaltic (A36 and A41) and microdioritic (A38 and A40) ballistic blocks, perhaps derived from explosions from different depths, might due to explosions intradiatreme (Valentine and White, 2012; Valentine *et al.*, 2015), fracturing the local aquifer to allow a new ascending body of basaltic

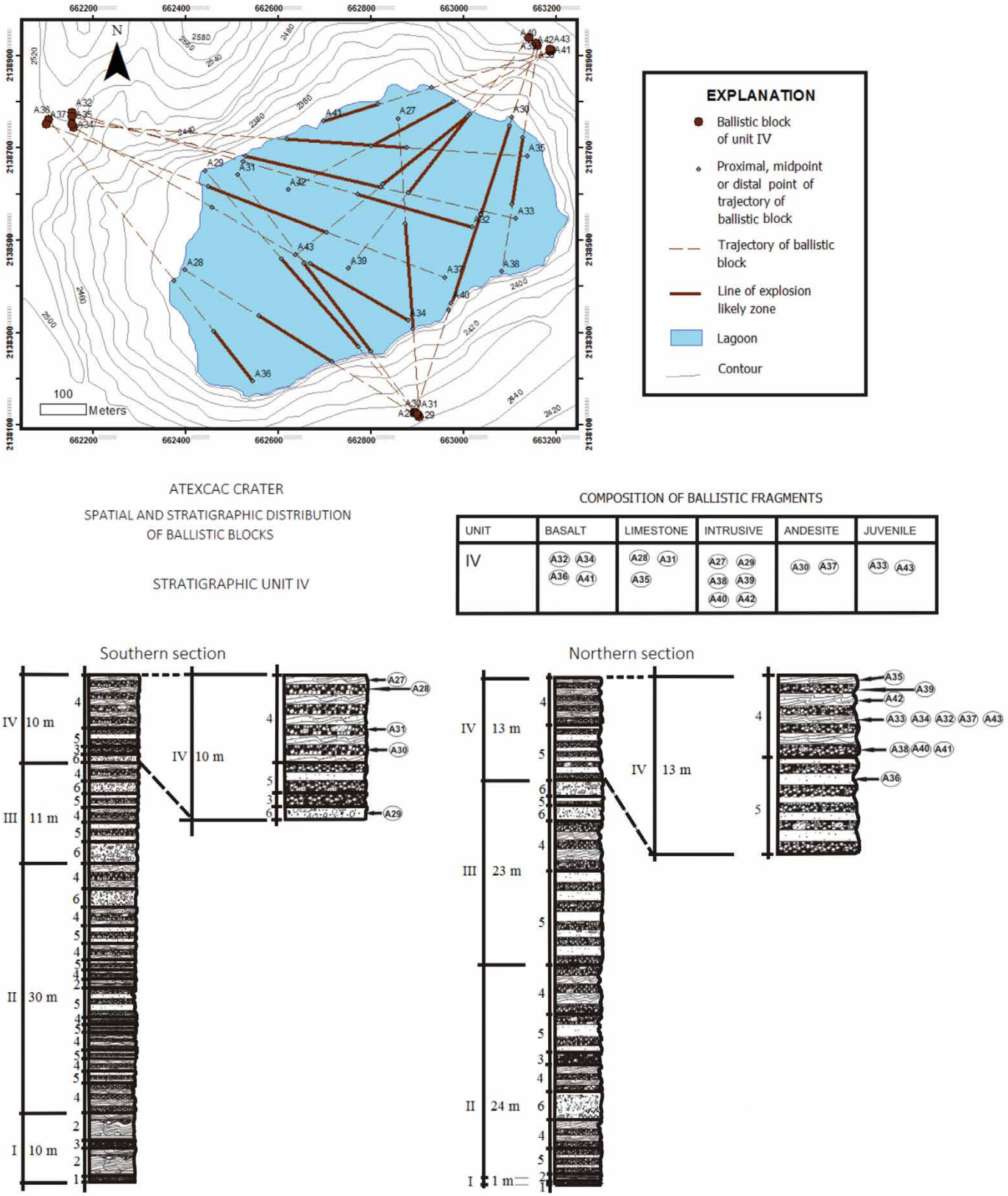

Figure 12. Map of spatial distribution and stratigraphic section of ballistic measured that occurred during the formation of unit IV and their respective composition. We can see chaotic orientations and alternation could be associated to the explosive locus during formation this stratigraphic unit. Brown thin dotted lines indicate directions of ballistics and thicker solid lines show likely explosion zones for each ballistic projectile.

Table 3. Composition, unit, facies type and explosive stage to which it belongs each of ballistic blocks considered in this study.

NUMBER	Composition	Stratigraphic unit	Type of facies	Explosive stage
A01	Basalt	I	2	1
A02	Basalt	I	2	1
A03	Andesite	I	2	1
A04	Basalt	I	2	1
A05	Basalt	I	2	1
A06	Microdiorite	I	3	1
A07	Basalt	I	2	1
A08	Microdiorite	I	2	1
A09	Microdiorite	I	2	1
A10	Limestone	I	2	1
A11	Basalt	I	2	1
A12	Basalt	II	4	2
A13	Microdiorite	II	4	2
A14	Limestone	II	4	2
A15	Microdiorite	II	4	2
A16	Limestone	II	5	2
A17	Microdiorite	II	4	2
A18	Basalt	II	5	2
A19	Microdiorite	II	4	2
A20	Limestone	II	4	2
A21	Microdiorite	II	5	2
A22	Basalt	II	4	2
A23	Microdiorite	II	6	2
A24	Andesite	II	4	3
A25	Limestone	II	4	3
A26	Andesite	II	4	3
A27	Microdiorite	IV	4	3
A28	Limestone	IV	4	3
A29	Microdiorite	IV	6	3
A30	Andesite	IV	5	3
A31	Limestone	IV	4	3
A32	Basalt	IV	4	3
A33	Juvenile	IV	4	3
A34	Basalt	IV	4	3
A35	Limestone	IV	4	3
A36	Basalt	IV	5	3
A37	Andesite	IV	4	3
A38	Microdiorite	IV	4	3
A39	Microdiorite	IV	4	3
A40	Microdiorite	IV	4	3
A41	Basalt	IV	4	3
A42	Microdiorite	IV	4	3
A43	Juvenile	IV	4	3

magma that interacted with the local aquifer, which in turn produce the deposition of surges and fallout layers (facies 4) at the crater´s southern and northern sectors. The location of the explosive locus was apparently simultaneous in all regions of the crater with diverse compositions of the ballistic blocks (basaltic, andesitic, microdioritic, limestone and juvenile material). At the upper part of last facies 4 of the maar sequence there are abundant accretionary lapilli and frequent bomb sags indicating wetter conditions and a new interaction with the aquifer. The directions of ballistic block shown their likely vent sources indicating, that they come from different explosive locus acting simultaneously. Another interesting characteristic worth to mention is the large variety of different lithologies of the present blocks during this stage (more microdiorite than basalt and limestone, but also andesite and juvenile) that could give support to the idea that the explosion locus occurred in distinct sites at same time and possibly at different depths, supporting the recent model proposed by Valentine and White (2012), in contrast to the traditional model proposed by Lorenz (1973, 1986). The morphology acquired by the crater, after of explosive stage 3, is basically the current morphology, but erosion and possibly rain removed materials with time collapsing and covering the western sector of the inner crater, and finally decreasing the lake area.

CONCLUSIONS

The depositional facies identified in the stratigraphic column of the Atexcac axalapazco indicate that the maar sequence was formed by phreatic, magmatic and phreatomagmatic explosions with intermittent interaction of ascendant magma bodies with the local aquifer due to fluctuations of availability of groundwater and this generated different conditions of wetness during the explosion phases. The analysis of depositional facies indicates that initial explosions occurred with very wet conditions (presence of accretionary lapilli), followed by a decrease of availability of groundwater with the ejection of the largest megablocks, mainly of microdioritic composition, and in the final phase, a new injection of basaltic magma was combined with sporadic wetter explosions with abundant presence of accretionary lapilli. The orientation of ballistic blocks and the resulting explosion zones suggest that the explosions started in the southwest sector and migrated to the northeast and then a more chaotic trend occurred with sometimes simultaneous active vents. This migration is far from being systematic, showing the occurrence of simultaneous explosions from different zones and perhaps from different depths.

In order to explain the evolution of the crater morphology we propose three explosives stages. An initial eruptive stage probably associated to the protodiatreme development (Valentine and White, 2012; Ross *et al.*, 2013) whose explosions occurred mainly along the southwest sector of the inner crater, followed by the eruptive stage 2 that caused crater widening to the northeast and a final eruptive stage with simultaneous and alternated explosive locus, producing facies deposits and ballistic blocks of various compositions that reflect a vertical mixing before ejecting of these blocks (Valentine and White, 2012; Valentine *et al.*, 2014), which in general originated the current morphology of crater.

The elongated shape of current crater of the Atexcac axalapazco could be associated to lateral migration of explosive epicenters (Valentine *et al.*, 2015) and it´s assumed that the maar-forming sequence was formed as a result of multiple subsurface explosions centered at different depths (White and Ross, 2011; Kereszturi and Németh, 2012; Valentine and White, 2012; Ross *et al.*, 2013; Valentine *et al.*, 2014; Valentine *et al.*, 2015). Although did not show a systematical lateral migration, it is evident a spatial and temporal migration of the explosion loci as the main control of the crater morphology. The variable location of vent sources proposed in this paper suggests an alternation of the explosive locus in different zones inside of crater. The study of ballistics may be a useful tool to analyze the evolution and morphology of a maar volcano like Atexcac and others in which there was a migration and/or alternation of the explosive locus.

ACKNOWLEDGEMENTS

This work was supported by CONACYT grant 15090 and PAPIIT IN-106314 and logistical support by Centro de Geociencias (UNAM).

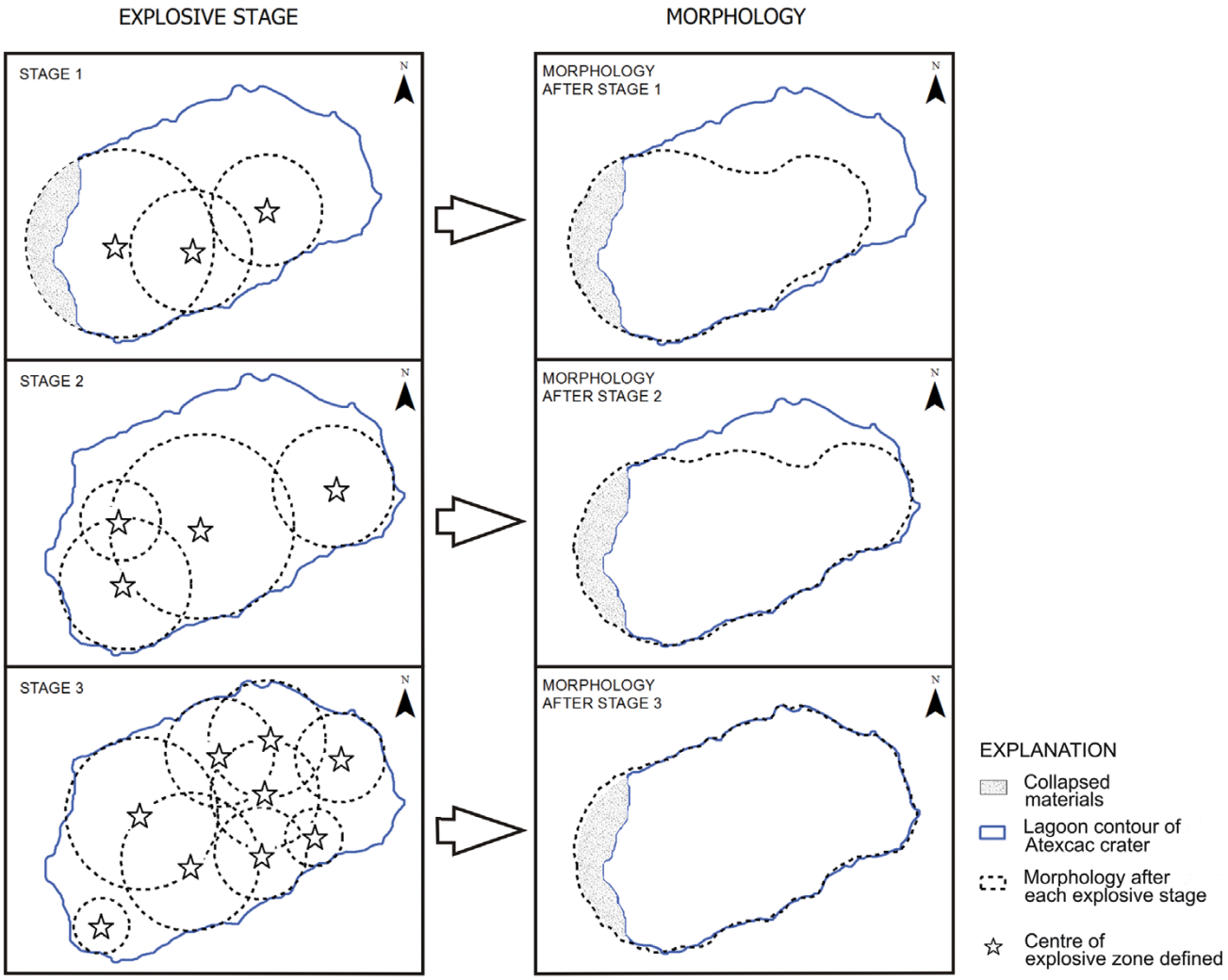

Figure 13. Scheme that show the relationship between each explosive stage and its respective morphology of crater. The explosions of stage 1 were located mainly a long of southwest sector of inner crater, the stage 2 caused a growing of crater to the northeast sector and the eruptive stage 3 that practically originated the current morphology of Atexcac crater.

Reviews by Karoly Nemeth were very useful for this work, as well as an anonymous reviewer. Gerardo Aguirre also provided some observations. We want to thank Lorena De León and Luis Rocha for help us in the field work. This paper was enriched by discussions with Michael Ort, Lorenz Volker and some other people that attended the field trip to the Serdán-Oriental area during the 5th International Maar Conference held at Queretaro in November 2015. Also, we appreciate the comments of Larry Mastin, Jacopo Taddeucci and Lionel Wilson that were very useful to improve this document.

REFERENCES

Austin-Erickson, A. 2007, Phreatomagmatic eruptions of rhyolitic magma: A case study of Tepexitl tuff ring, Serdan-Oriental basin, Mexico: Texas, U.S.A., Northern Arizona University, Flagstaff, MS thesis, 194 pp.

Austin-Erickson, A., Büttner, R., Dellino, P., Ort, M.H., Zimanowski, B., 2008, Phreatomagmatic explosions of rhyolitic magma: Experimental and field evidence: Journal of Geophysical Research, 113, B11201, doi:10.1029/2008JB005731.

Austin-Erickson, A., Ort, M.H., Carrasco-Núñez, G., 2011, Rhyolitic phreatomagmatism explored: Tepexitl tuff ring (Eastern Mexican Volcanic Belt): Journal of Volcanology and Geothermal Research, 201, 325-341.

Alatorre-Ibargüengoitia, M.A., Delgado-Granados, H., 2006, Experimental determination of drag coefficient for volcanic materials: Calibration and application of a model to Popocatépetl volcano (Mexico) ballistic projectiles: Geophysical Research Letters, 33, L11302. doi:10.1029/2006GL026195.

Bower, S.M., Woods, A.W., 1996, On the dispersal of clasts from volcanic craters during small explosive eruptions: Journal of Volcanology and Geothermal Research, 73, 19-32.

Büttner, R., Dellino, P., La Volpe, L., Lorenz, V., Zimanowski, B., 2002, Thermohydraulic explosions in phreatomagmatic eruptions as evidenced by comparision between pyroclasts and products from Molten Fuel Interaction experiments: Journal of Geophysical Research, 107, (B11), 2277, doi:10.1029/2001JB000511.

Carrasco-Núñez, G., Riggs, N.R., 2008, Polygenetic nature of a rhyolitic dome and implications for hazard assessment: Cerro Pizarro volcano, Mexico: Journal of Volcanology and Geothermal Research, 171, 307-315.

Carrasco-Núñez, G., Ort, M., Romero, C., 2007, Evolution and hydrological conditions of a maar volcano (Atexcac crater, Eastern Mexico): Journal of Volcanology and Geothermal Research, 159, 179-197.

Donnadieu, F., Dubosclard, G., Cordesses, R., Druitt, T., Hervier, C., Kornprobst, J., Lénat, J.F., Allard, P., Coltelli, C., 2005, Remotely monitoring volcanic activity with ground-based Doppler radar: Eos, 86 (21), 201-204.

Fagents, S.A., Wilson, L., 1993, Explosive volcanic eruptions- VII. The ranges of pyroclasts ejected in transient volcanic explosions: Geophysical Journal International, 113, 359-370.

Fisher, R.V., Schmincke, H.U., 1984, Pyroclastic Rocks: New York, Springer, 472 p.

Fisher, R.V., Waters, A.C., 1970, Base surge bed forms in maar volcanoes: American Journal Science, 268, 157-180.

Fudali, R.F., Melson, W.G., 1972, Ejecta velocities, magma chamber pressure and kinetic energy associated with the 1968 eruption of Arenal volcano: Bulletin of Volcanology, 35, 383-401.

Gasca-Durán, A., 1981, Génesis de los lagos-cráter de la cuenca de Oriental: Colección Científica Prehistórica, 98, 57 p.

Gouhier, M., Donnadieu, F., 2011, Systematic retrieval of ejecta velocities and gas fluxes at Etna volcano using L-Band Doppler radar: Bulletin of Volcanology, 73, 1139-1145.

Ishihara, K., 1985, Dynamical analysis of volcanic explosion: Journal of Geodynamics, 3, 327-349.

Jordan, S.C., Cas, R.A.F., Hayman, P.C., 2013, The origin of a large (>3 km) maar volcano by coalescence of multiple shallow craters: Lake Purrumbete maar, southeastern Australia: Journal of Volcanology and Geothermal Research, 254, 5-22.

Kereszturi, G., Németh, K, 2012, Monogenetic Basaltic Volcanoes: Genetic Classification, Growth, Geomorphology and Degradation, Chapter 1, *en* Németh, K. (ed.) Updates in Volcanology - New Advances in Understanding Volcanic Systems: InTech, open acces article, http://dx.doi.org/10.5772/51387, ISBN: 978-953-51-0915-0.

Kienle, J., Kyle, P.R., Self, S., Motyka, R., Lorenz, V., 1980, Ukinrek Maars, Alaska, I. Eruption sequence, petrology and tectonic setting: Journal of Volcanology and Geothermal Research, 7, 11-37.

Lorenz V., 1973, On the formation of Maars: Bulletin of Volcanology, 37, 183-204.

Lorenz, V., 1986, On the growth of maars and diatremes and its relevance to the formation of tuff rings: Bulletin of Volcanology, 48, 265-274.

Lorenz, V., 2003, Maar–diatreme volcanoes, their formation, and their setting in hard rock or soft rock environments: Geolines, 15, 72-83.

Lorenz, V., 2007, Syn- and posteruptive hazard of maar-diatreme volcanoes: Journal of Volcanology and Geothermal Research, 159, 285-312.

Lorenz, V., Zimanowski, B., Büttner, R., 2002, On the formation of deep-seated subterranean peperita-like magma-sediment mixtures: Journal of Volcanology and Geothermal Research, 114, 107-118.

Mastin, L., 2008, A simple calculator of ballistics trajectories for blocks ejected during volcanic eruptions, version 1.4: United States Geological Survey Open File Report, 01-45.

McGetchin, T.R., Settle, M., Chouet, B.A., 1974, Cinder cone growth modeled after Northeast Crater, Mount Etna, Sicily: Journal of Geophysical Research, 79 (23), 3257-3272.

Minakami, T, 1942, On the distribution of volcanic ejecta (Part I): The distributions of volcanic bombs ejected by recent explosions of Asama: Bulletin of Earthquake Research Institute, 20, 65-92.

Mironer, A., 1979, Engineering fluid mechanics: New York, McGraw-Hill, 592 pp.

Nairn, I. A., 1976, Atmospheric shock waves and condensation clouds from Ngauruhoe explosive eruptions: Nature, 259, 190-192.

Nairn, I.A., Self, S., 1978, Explosive eruptions and pyroclastic avalanches from Ngauruhoe in February 1975: Journal of Volcanology and Geothermal Research, 3, 39-60.

Németh, K, Martin, U, Harangi, Sz, 2001, Miocene phreatomagmatic volcanism at Tihany (Pannonian Basin, Hungary): Journal of Volcanology and Geothermal Research, 111, 111-135.

Ollier, C.D., 1967, Maars, their characteristics, varieties and definition: Bulletin of Volcanology, 31, 45-73.

Ort, M., Carrasco-Núñez, G., 2009, Lateral vent migration during phreatomagmatic and magmatic eruptions at Tecuitlapa maar, east-central Mexico: Journal of Volcanology and Geothermal Research, 181, 67-77.

Pfeiffer, T, 2001, Vent development during the Minoan eruption (1640 BC) of Santorini, Greece, as suggested by ballistic blocks: Journal of Volcanology and Geothermal Research, 106, 229-242.

Riggs, N.R., Carrasco-Núñez, G., 2004, Evolution of a complex, isolated dome system, Cerro Pizarro, central Mexico: Bulletin of Volcanology, 66, 322-335.

Ross, P.S., White, J.D.L., 2006, Debris jets in continental phreatomagmatic volcanoes: a field study of their subterranean deposits in the Coombs Hills vent complex, Antarctica: Journal of Volcanology and Geothermal Research, 149, 62-84.

Ross, P.S., White, J.D.L., Valentine, G.A., Taddeucci, J. Sonder, I., Andrews. R.G., 2013, Experimental birth of a maar–diatreme volcano: Journal of Volcanology and Geothermal Research, 260, 1-12.

Rosseel, J.B., White, J.D.L., Houghton, B.F., 2006, Complex bombs of phreatomagmatic eruptions: Role of agglomeration and welding in vents of the 1886 Rotomahana eruption, Tarawera, New Zealand: Journal of Geophysical Research, 111, B12205, doi:10.1029/2005JB004073.

Self, S., Kienle, J., Huot, J.P., 1980, Ukinrek maars, Alaska, II, deposits and formation of the 1977 craters: Journal of Volcanology and Geothermal Research, 7, 39-65.

Sherwood, A.E., 1967, Effect of air drag on particles ejected during explosive cratering: Journal of Geophysical Research, 72, 1783-1791.

Sohn, Y.K., 1996, Hydrovolcanic processes forming basaltic tuff rings and cones on Cheju Island, Korea: Geological Society American Bulletin, 108(10), 1199-211.

Swanson, D.A., Zolkos, S.P, Haravitch, B., 2012, Ballistic blocks around Kilauea Caldera: Their vent locations and number of eruptions in the late 18th century: Journal of Volcanology and Geothermal Research, 231, 1-11.

Taddeucci, J., Scarlato, P., Capponi, A., Del Bello, E., Cimarelli, C., Palladino, D.M., Kueppers, U., 2012, High-speed imaging of Strombolian explosions: The ejection velocity of pyroclasts: Geophysical Research Letters, 39, L02301, doi:10.1029/2011GL050404.

Taddeucci, J., Sesterhenn, J., Scarlato, P., Stampka, K., Del Bello, E., Pena-Fernandez, J.J., Gaudin, D., 2014, Highspeed imaging, acoustic features, and aeroacoustic computations of jet noise from Strombolian (and Vulcanian) explosions: Geophysical Research Letters, 41, 3096-3102, doi:10.1002/2014GL059925.

Valentine, G.A., White, J.D.L., 2012, Revised conceptual model for maar-diatremes: Subsurface processes, energetics, and eruptive products: Geology, 40, 1111-1114.

Valentine, G.A., Shufelt, N.L., Hintz, A.R.L., 2011, Models of maar volcanoes, Lunar Crater (Nevada, USA): Bulletin of Volcanology, 73, 753-765.

Valentine, G.A., Graettinger, A.H., Sonder I., 2014, Explosion depths for phreatomagmatic eruptions: Geophysical Research Letters, 41, 3045-3051, DOI 10.1002/2014GL060096.

Valentine, G.A., Graettinger, A.H., Macorps, E., Ross, P.S., White, J.D.L., Döhring, E., Sonder I., 2015, Experiments with vertically and laterally migrating subsurface explosions with applications to the geology of phreatomagmatic and hydrothermal explosion craters and diatremes: Bulletin of Volcanology, 77, 15, 1-17, DOI 10.1007/s00445-015-0901-7.

Waitt, R.B., Mastin, L.G., Miller, T.P., 1995, Ballistic showers during Crater Peak eruptions of Mount Spurr Volcano, summer 1992: United States Geological Survey Bulletin, 2139, 89-106.

White, J.D.L., Ross, P.S, 2011, Maar-diatreme volcanoes: A review: Journal of Volcanology and Geothermal Research, 201, 1-29.

White, J.D.L., Schmincke, H.U., 1999, Phreatomagmatic eruptive and depositional processes during the 1949 eruption on La Palma (Canary Islands): Journal of Volcanology and Geothermal Research, 94, 283-304.

Wilson, L., 1972, Explosive volcanic eruptions II, the atmospheric trajectories of pyroclasts: Geophysical Journal of the Royal Astronomical Society (London), 30, 381-392.

Wohletz, K.H., 1986, Explosive magma-water interactions: Thermodynamics, explosion mechanisms, and field studies: Bulletin of Volcanology, 48, 245-264.

Wohletz, K.H., Sheridan, M.F., 1983, Hydrovolcanic explosions II. Evolution of basaltic tuff rings and tuff cones: American Journal of Science, 283, 385-413.

Yáñez, C., García, S., 1982, Exploración geotérmica de la región geotérmica Los Humeros-Las Derrumbadas, Estados de Puebla y Veracruz, C.F.E., 96p.

Zimanowski, B., Büttner, R., Lorenz, V., 1997, Premixing of magma and water in MFCI experiments: Bulletin of Volcanology, 68, 419-495.

Zimmer, B.W., Riggs, N.R., Carrasco-Núñez, G., 2010, Evolution of tuff ring-dome complex: the case study of Cerro Pinto, eastern Trans-Mexican Volcanic Belt: Bulletin of Volcanology, 72, 1223-1240.

Manuscript received: February 27, 2015
Corrected manuscript received: August 28, 2015
Manuscript accepted: August 31, 2015